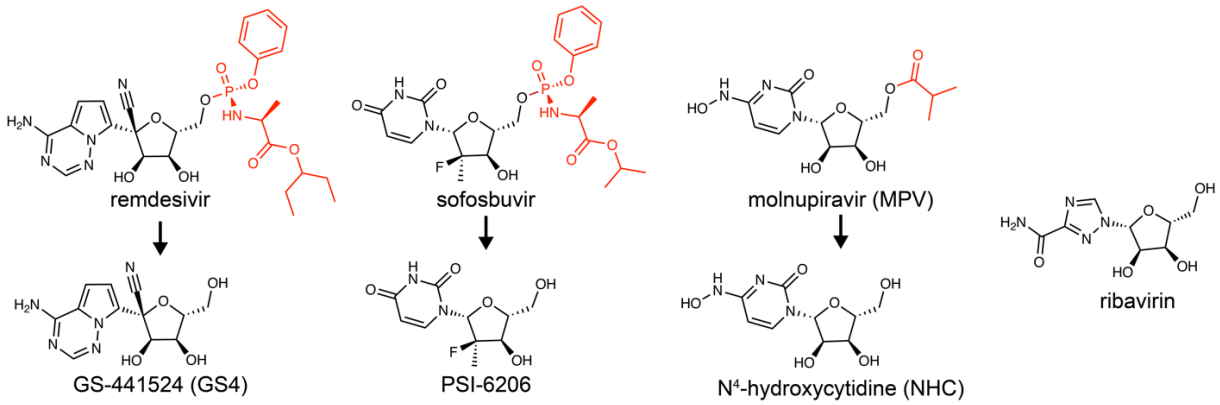

Supplementary Figure 1 | Chemical structures of nucleoside-analogue antivirals and their prodrug precursors.

Chemical structures of remdesivir, sofosbuvir, and molnupiravir, with their respective parent nucleosides (GS4, PSI-6206, and NHC) shown at bottom. 5' protecting groups depicted in red. Nucleoside analogue ribavirin shown at right.

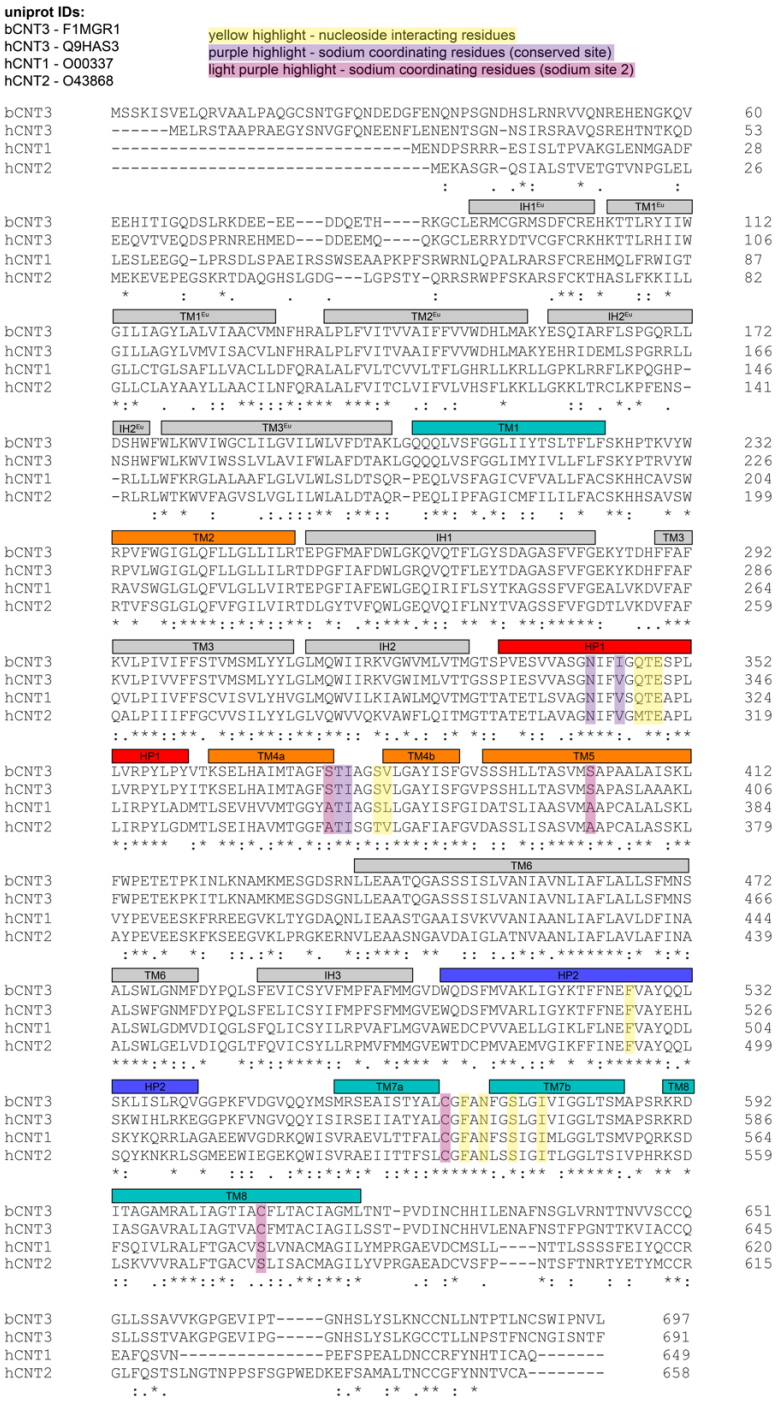

Supplementary Figure 2 | Multiple sequence alignment of select concentrative nucleoside transporters.

Multiple sequence alignment of *Bos taurus* CNT3 and human CNT isoforms 1-3. Residues involved in nucleoside coordination are highlighted in yellow; residues comprising the "conserved sodium site" (site 1) are highlighted in purple; residues comprising the "sodium site 2" are highlighted in light purple. Uniprot IDs associated with each sequence shown at top left.

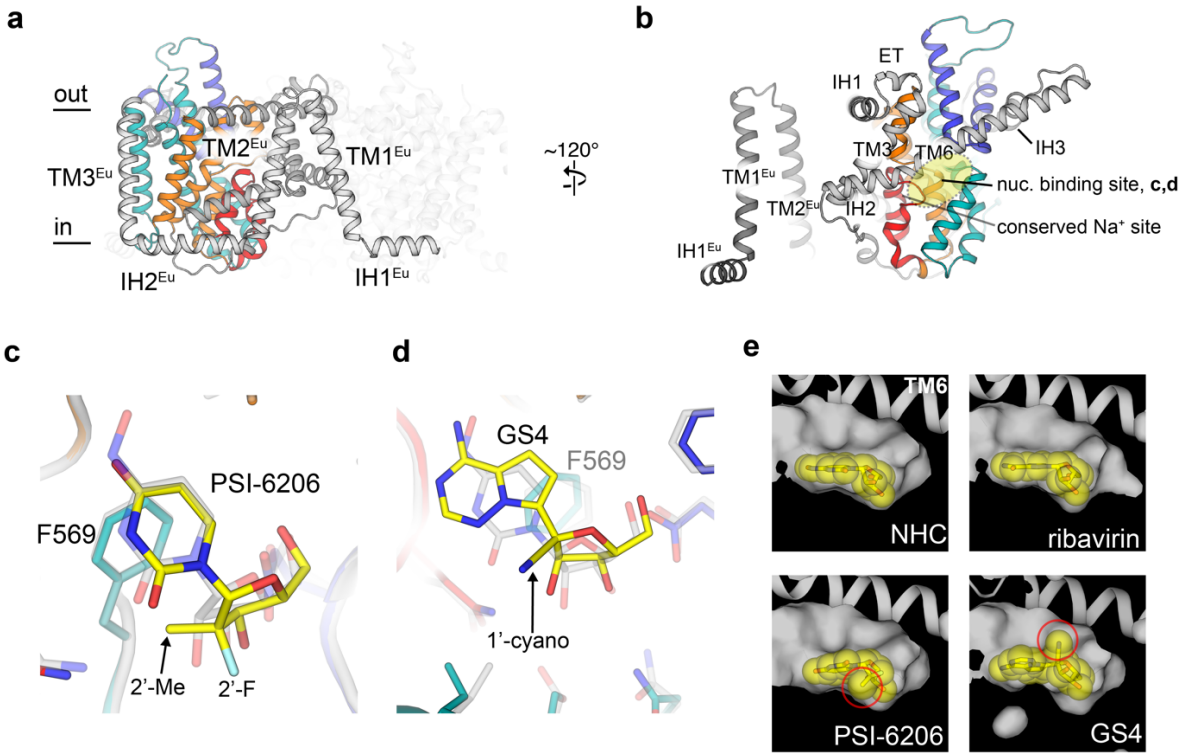

Supplementary Figure 3 | Inward-facing bCNT3 in apo and antiviral drug bound states.

a, Overall transporter architecture, with the eukaryotic scaffold domain emphasized. **b**, Overall architecture of the conserved CNT fold. **c**, Zoomed in view of the 2' position of ribose in the PSI-6206 structure, with the NHC structure superposed and shown in transparent grey for reference. **d**, Zoomed-in view of the 1' position of ribose in the GS4 structure, with the NHC structure superposed and shown in transparent grey for reference. **e**, Nucleoside binding pocket all four drug-bound structures, with bulky ribose substituents of PSI-6206 and GS4 circled. TM6 of the scaffold domain shown as cartoon for reference.

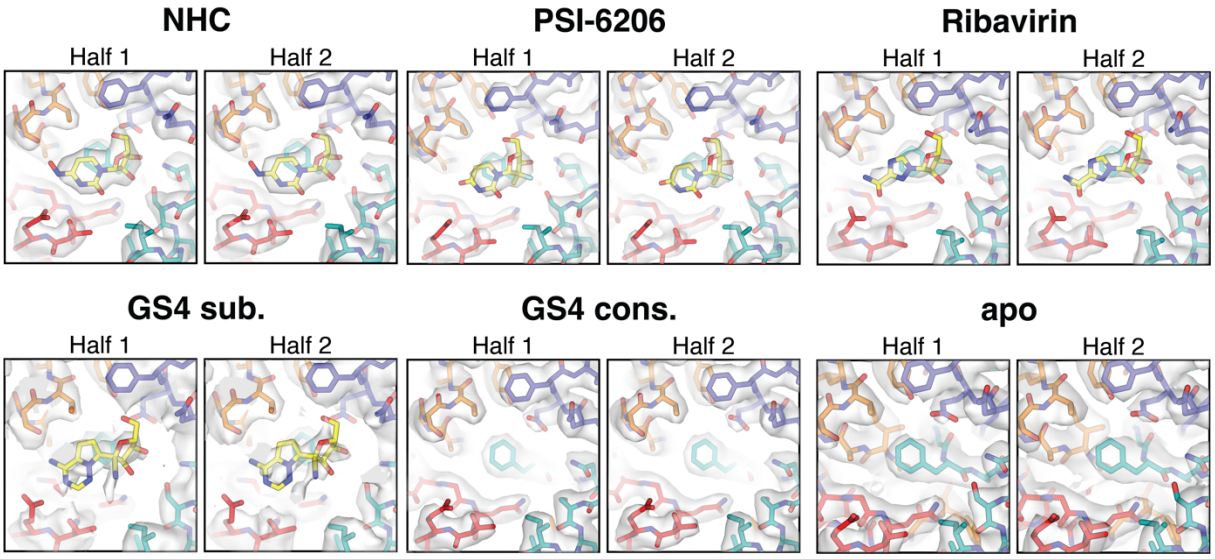

Supplementary Figure 4 | Cryo-EM half maps for CNT3 substrate binding pocket.

Local cryo-EM half map reconstructions for CNT3 substrate binding pocket. Cryo-EM densities are shown at map threshold values of 6σ for NHC, PSI-6206, ribavirin, GS4 sub., apo, or 7σ for GS4 cons.

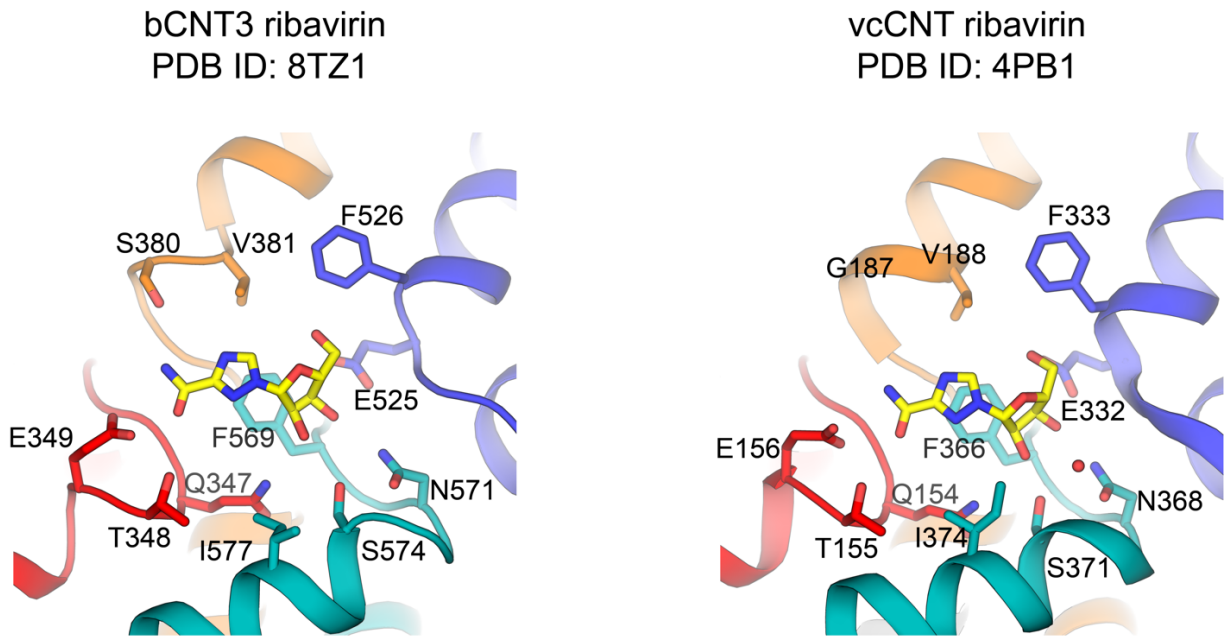

Supplementary Figure 5 | Comparison of ribavirin bound to eukaryotic or bacterial CNT.

Protein ligand interactions for ribavirin complexed to bCNT3 in the cryo-EM structure (left, this study) and ribavirin complexed to the bacterial CNT vcCNT in the X-ray crystal structure (right, previous study[20]).

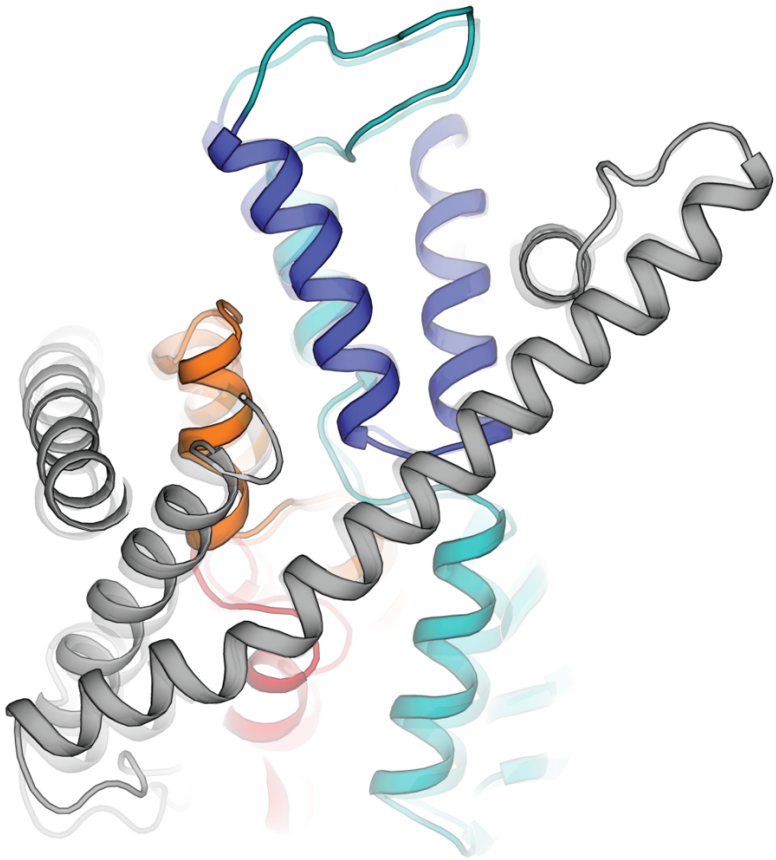

Supplementary Figure 6 | MD transition of INT1 to IFS state.

Final normal MD frame (500 ns) of NHC-bound INT1 structure (solid) overlayed with experimental IFS structure (transparent), showing final structural transition from INT1 to IFS states.

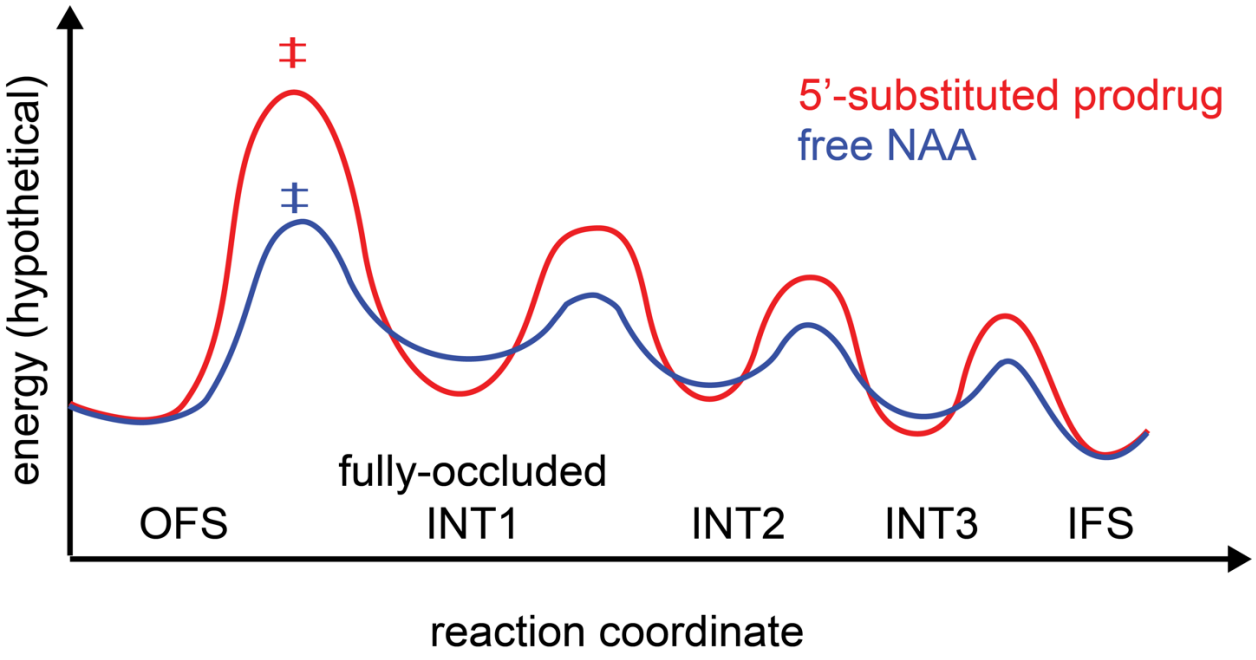

Supplementary Figure 7 | Hypothetical energetic landscapes.

Transition of elevator-type motion of CNT3 from OFS to IFS in the presence of free NAA or 5’-substituted prodrug. 5’-substituted prodrug may elevate the energetic barrier between the states or stabilize individual states. The isomerization from OFS to INT1 likely represents the highest energy barrier during translocation (transition state of this conversion denoted with *‡).*

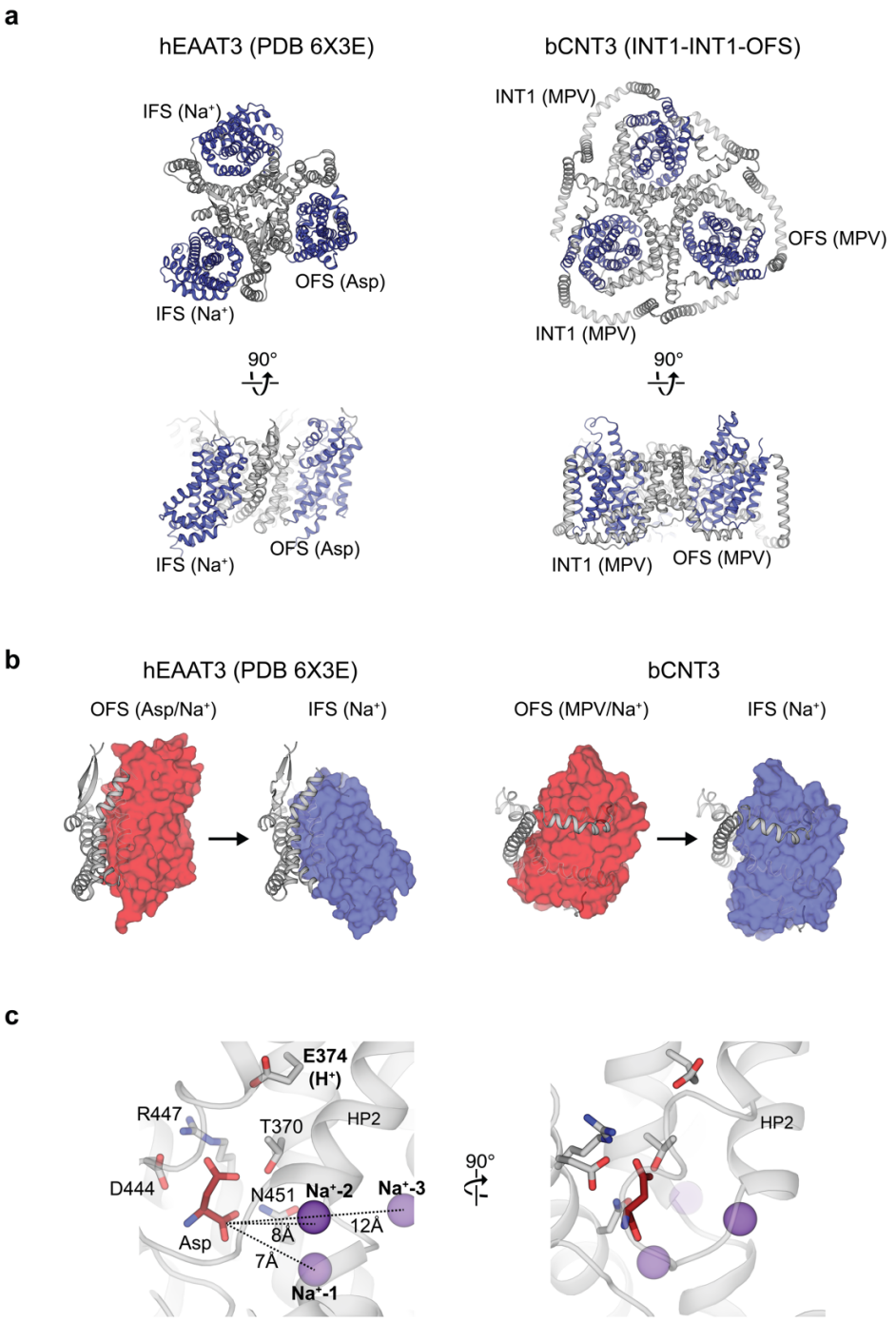

Supplementary Figure 8 | Comparison of bCNT3 with representative SLC1 member hEAAT3.

a, Top-down and side view of IFS-IFS-OFS hEAAT3 (previous study[44]; PDB 6X3E) and INT1-INT1-OFS bCNT3 (this study; PDB 8TZD). Transport domain colored in blue, scaffold domain colored in grey. **b**, Comparison of the transport domain movements between the two end states (OFS and IFS) in SLC1 and SLC28. Transport domain depicted as colored surface (red – OFS, blue – IFS) and scaffold domain colored in grey. **c**, The arrangement of substrate and co-transported ions in the hEAAT3 substrate binding pocket.

	apo (EMD-41731) (PDB 8TZ2)	NHC (EMD-41734) (PDB 8TZ5)	PSI-6206 (EMD-41735) (PDB 8TZ6)	ribavirin (EMD-41730) (PDB 8TZ1)	GS4 cons. (EMD-41732) (PDB 8TZ3)	GS4 sub. (EMD-41733) (PDB 8TZ4)
Data collection and processing					**dataset: GS-441524**	
Magnification	81,000	81,000	81,000	81,000	81,000	
Voltage (kV)	300	300	300	300	300	
Electron exposure (e–/Å^2)	60	60	60	60	50	
Defocus range (μm)	-0.8 to -1.8	-1.0 to -2.25	-0.8 to -1.8	-0.8 to -1.8	-1.0 to -2.0	
Pixel size (Å)	1.08	1.12	1.08	1.08	1.08	
Symmetry imposed	C3	C3	C3	C3	C3	C1
Initial particle images (no.)	2,186,756	1,687,435	2,827,294	2,714,156	3,586,285	
Final particle images (no.)	102,248	147,332	199,596	247,980	498,109	38,774
Map resolution (Å) (FSC threshold=0.143)	2.80	2.74	2.69	2.54	2.31	3.23
Refinement						
Initial model used	GS4 cons.	GS4 cons.	GS4 cons.	GS4 cons.	PDB:3TIJ	GS4 cons.
Map sharpening *B* factor (Å^2)	100.2	104.9	96.0	50.0	89.8	86.2
Model composition						
Non-hydrogen atoms	24,828	25,395	25,398	25,398	25,320	24,4421
Protein residues	1,599	1,599	1,599	1,599	1,599	1,599
Ligands	LBN: 6, NA: 6	NA:3, U56:3, LBN: 12	NA:3, U7I:3, LBN:12	NA:6, RBV:3, LBN:12	NA:6, LBN:12	U08:1
B factors (Å^2)						
Protein	41.70	48.37	56.17	86.33	36.60	63.19
Ligand	43.04	52.26	56.23	87.10	37.21	44.46
R.m.s. deviations						
Bond lengths (Å)	0.004	0.002	0.004	0.003	0.008	0.002
Bond angles (°)	0.551	0.440	0.511	0.465	0.681	0.407
Validation						
MolProbity score	0.95	0.94	1.02	0.89	1.13	0.96
Clashscore	1.90	1.44	2.35	1.48	1.92	1.96
Poor rotamers (%)	0.00	0.24	0.48	0.48	0.00	0.00
Ramachandran plot						
Favored (%)	98.87	97.74	98.12	99.06	96.99	99.12
Allowed (%)	1.13	2.26	1.88	0.94	2.82	0.88
Disallowed (%)	0.00	0.00	0.00	0.00	0.19	0.00

Supplementary Table 1 | Cryo-EM data collection, refinement, and validation statistics (part 1)

	apo	NHC	PSI	Rib	GS4 Sub
apo	-	0.123	0.1072	0.1070	0.1138
NHC		**0.8317**			
PSI			**0.7903**		
Rib				**0.8663**	
GS4 sub					**0.7106**

Supplementary Table 2 | Local pairwise cross correlation values for apo and liganded structures.

Map-to-map cross-correlation values for liganded structure-liganded map (self-correlation) and liganded structures against apo map. The cross-correlation values are calculated using Chimera by generating a map from PDB coordinates using only respective ligands followed by cross correlation calculation of the generated ligand map against experimental map.

	INT1-INT1-OFS (EMD-41755) (PDB 8TZD)	INT1 (C3) (EMD-41736) (PDB 8TZ7)	INT1-INT1-INT3 (EMD-41737) (PDB 8TZ8)	INT2 (C3) (EMD-41738) (PDB 8TZ9)	INT1-INT1-INT2 (EMD-41739) (PDB 8TZA)
Data collection and processing	**dataset: MPV condition 1**			**dataset: MPV condition 2**	
Magnification	81,000			81,000	
Voltage (kV)	300			300	
Electron exposure (e–/Å^2)	60			60	
Defocus range (μm)	-0.8 to -1.8			-0.8 to -1.8	
Pixel size (Å)	1.08			1.08	
Symmetry imposed	C1	C3	C1	C3	C1
Initial particle images (no.)	2,592,142			2,026,720	
Final particle images (no.)	118,133	127,798	109,039	4,412	15,400
Map resolution (Å) (FSC threshold=0.143)	3.20	3.00	3.19	3.67	3.43
Refinement					
Initial model used	GS4 cons.	GS4 cons.	GS4 cons.	GS4 cons.	GS4 cons.
Map sharpening *B* factor (Å^2)	98.0	113.0	95.7	59.5	63.0
Model composition					
Non-hydrogen atoms	24,197	24,615	24,586	24,354	24,354
Protein residues	1,587	1,599	1,599	1,599	1,599
Ligands	XMO:3, LBN:1	XMO:3, LBN:3	XMO:3, LBN:2	XMO:3	XMO:3
B factors (Å^2)					
Protein	39.63	57.48	60.42	89.01	60.33
Ligand	27.52	60.04	58.09	69.19	44.47
R.m.s. deviations					
Bond lengths (Å)	0.004	0.003	0.004	0.003	0.002
Bond angles (°)	0.932	0.465	0.494	0.551	0.445
Validation					
MolProbity score	1.24	1.01	1.19	1.17	1.04
Clashscore	4.72	2.29	4.00	3.87	2.55
Poor rotamers (%)	0.16	0.24	0.00	0.72	0.00
Ramachandran plot					
Favored (%)	98.23	98.31	98.31	98.31	99.00
Allowed (%)	1.77	1.69	1.69	1.69	1.00
Disallowed (%)	0.00	0.00	0.00	0.00	0.00

Supplementary Table 3 | Cryo-EM data collection, refinement, and validation statistics (part 2)

System Name	# of atoms	Replicas	# of Ions (Na^+/Cl^-)	Simulation time (ns)
NHC	244964	5	144/176	500
MPV	239698	5	139/171	500
NHC-SMD	238701	1	137/169	15
MPV-SMD	240259	1	139/171	15

Supplementary Table 4 | MD simulation system setup.

Lipid name	% lipids within each leaflet	
	Outer	Inner
1-palmitoyl-2-oleoyl-sn-phosphatidylcholine	45	60
N-stearoyl-D-erythro-sphingosylphosphorylcholine	22	10
Cholestrol	33	30

Supplementary Table 5 | Lipid composition in MD simulations.